Generating microstructures with specified correlation functions

N. Sheehan
Department of Chemical Engineering, Princeton University, Princeton, New Jersey 08544

S. Torquato[a)]
Department of Chemistry and the Princeton Materials Institute, Princeton University, Princeton, New Jersey 08544

(Received 17 July 2000; accepted for publication 28 September 2000)

A stochastic optimization technique has recently been developed that can reconstruct or construct random heterogeneous materials with specified statistical correlation functions. We demonstrate how this technique can be used to reconstruct a digitized image of an interpenetrating, isotropic ceramic-metal composite. In this case, the two-point probability function displays no short-range order and the image is reconstructed by optimizing in two orthogonal directions only. However, this technique results in artificial anisotropy in the unoptimized directions when one (re)constructs an image in which the isotropic two-point probability function exhibits appreciable short-range order. We show that by optimizing in more than two directions, one can effectively eliminate the artificial anisotropic effects for a system possessing significant short-range order. This is done by optimizing in three directions on a hexagonal grid and by optimizing in four directions on a square grid. Finally, an aspect of the nonuniqueness of the resulting structures is quantitatively examined. © *2001 American Institute of Physics.* [DOI: 10.1063/1.1327609]

I. INTRODUCTION

The challenge of reconstructing microstructural images of heterogeneous materials from limited microstructural information is an interesting and important problem.[1–8] Such reconstructions can give insight into the information contained in a microstructural image by determining the minimum set of correlation functions necessary to reconstruct an image. Another interesting question concerns how to quantify the nonuniqueness of the reconstructed images. A very practical benefit of the reconstruction procedure could be the identification of the classes of three-dimensional microstructures that can be reconstructed from only two-dimensional (2D) planar cuts through the material. A different but interesting exercise involves constructing images with a given set of hypothetical correlation functions. This study can lead to a more thorough understanding of the properties of physically realizable correlation functions and limitations of the reconstruction technique.

There are two basic techniques available for these (re-)constructions. One commonly used method is based on the use of Gaussian random fields.[1–3] More recently, a simulated-annealing technique was introduced by Rintoul and Torquato[4] to reconstruct molecular systems. Yeong and Torquato[5,6] extended this method to reconstruct digitized heterogeneous media. To implement this technique, one starts with a given, arbitrarily chosen, initial configuration of ''black'' and ''white'' pixels and a set of *reference* or *target* correlation functions. The ''energy'' is defined as a functional of the squared difference between the simulated and target correlation functions at any instant of time. By interchanging black and white pixels, the energy is minimized via the simulated annealing method.

In this article, we explore better ways to sample for the statistical correlation functions of interest using the Yeong–Torquato method for digitized media. Various sampling methods have been employed. One approach utilizes an efficient fast Fourier transform[7] to sample for the standard two-point probability function. This technique samples for this function in every direction on the lattice and hence, at the end of the optimization process, matches (or *optimizes*) the correlation function in every direction. The disadvantage of this technique is that it is limited only to the two-point probability function, which is insufficient to reconstruct certain images. The Yeong–Torquato method is a general technique, as it allows any number and type of microstructural descriptors to be incorporated into the optimization routine. To minimize computational cost, they sampled the microstructural descriptors only along the orthogonal lattice directions.[5,6] Cule and Torquato[7] showed that this technique is successful, provided that the system size is much larger than the correlation length of the function(s) being optimized. However, they also showed that if this condition is not met, then orthogonal sampling can lead to artificial anisotropy in the unoptimized directions. This last point was also observed by Manwart and Hilfer.[8]

The rest of the article is laid out as follows. In Sec. III, the microstructural descriptors used in the reconstruction algorithm are described. The simulated annealing algorithm is then described in Sec. IV. In Sec. V, we reconstruct an actual image of a ceramic-metal composite from its two-point probability function to demonstrate the effectiveness of the orthogonal sampling technique when no short-range order ex-

[a)]Author to whom correspondence should be addressed; electronic mail: torquato@princeton.edu

ists. In Sec. VI, a construction is presented for a two-point probability function displaying appreciable short-range order. The construction shows how the orthogonal sampling technique, in this case, results in an image which displays artificial anisotropy in the unoptimized directions. We then introduce an improvement on this algorithm by optimizing in more than two directions and demonstrate how this improved technique significantly reduces the anisotropy. In Sec. VII, the issue of nonuniqueness of reconstructed images is further explored.

II. DESCRIPTORS OF RANDOM MEDIA

The indicator function $I^{(i)}(\mathbf{x})$ for phase i in a two-phase random medium is defined by

$$I^{(i)}(\mathbf{x})=\begin{cases}1 & \text{if } \mathbf{x} \text{ lies in phase } i,\\ 0 & \text{otherwise.}\end{cases} \tag{1}$$

The n-point correlation (or probability) function $S_n^{(i)}$ is defined as

$$S_n^{(i)}(\mathbf{x}_1,\mathbf{x}_2,\ldots,\mathbf{x}_n)=\langle I^{(i)}(\mathbf{x}_1)I^{(i)}(\mathbf{x}_2)\ldots I^{(i)}(\mathbf{x}_n)\rangle, \tag{2}$$

where angular brackets denote an ensemble average. The quantity $S_n^{(i)}(\mathbf{x}_1,\mathbf{x}_2,\ldots,\mathbf{x}_n)$ gives the probability that n points located at positions $\mathbf{x}_1$, $\mathbf{x}_2,\ldots,\mathbf{x}_n$ all lie in the same phase i.

If the medium is statistically homogeneous then $S_n^{(i)}$ is translationally invariant, depending on the relative displacements $\mathbf{x}_2-\mathbf{x}_1$, $\mathbf{x}_3-\mathbf{x}_1,\ldots,\mathbf{x}_n-\mathbf{x}_1$. For example, the one-point function is simply given by the constant volume fraction of phase i, i.e.,

$$S_1^{(i)}=\langle I^{(i)}(\mathbf{x})\rangle=\phi_i. \tag{3}$$

The two-point probability function, also known as the autocorrelation function, is given by

$$S_2^{(i)}(\mathbf{r})=\langle I^{(i)}(\mathbf{x}_1)I^{(i)}(\mathbf{x}_2)\rangle, \tag{4}$$

where $\mathbf{r}=\mathbf{x}_2-\mathbf{x}_1$ and, at it extreme values is given by

$$0\leqslant S_2(\mathbf{r})\leqslant\phi_1, \tag{5}$$

assuming no long-range order. Under the ergodic hypothesis, the ensemble average earlier can be replaced by a volume average in the limit that the volume tends to infinity, i.e.,

$$S_2^{(i)}(\mathbf{r})=\lim_{V\to\infty}\frac{1}{V}\int_V I^{(i)}(\mathbf{y})I^{(i)}(\mathbf{y}+\mathbf{r})d\mathbf{y}. \tag{6}$$

For statistically isotropic media, $S_2^{(i)}(r)$ depends only on the distance $r=|\mathbf{r}|$. Hereafter, we will drop the superscript i and refer to $S_2(r)$ as the autocorrelation function of phase 1. In general, S_2 obeys the elementary bounds $0\leqslant S_2\leqslant\phi_1$.

Integral positivity conditions for the autocorrelation function have recently been studied.[9] The positivity conditions allow one to check if the autocorrelation function is physically realizable. For isotropic media in d dimensions, there are actually d positivity conditions. The conditions that apply for isotropic two-dimensional systems are

$$\int_0^\infty\gamma(r)\cos(kr)dr\geqslant 0 \quad \forall k, \tag{7}$$

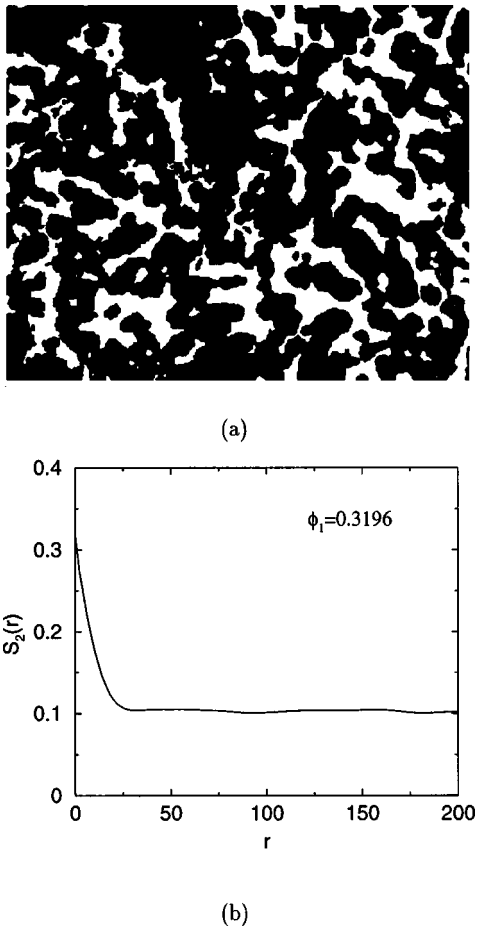

FIG. 1. (a) Microstructural image of a ceramic-metal composite. The white areas (phase 1) are aluminum and the black areas (phase 2) are mainly a the ceramic phase composed of boron carbide. (b) Autocorrelation function for the white phase of the ceramic-metal composite. The function displays no appreciable short-range order, so it is suitable for reconstruction using orthogonal sampling techniques.

$$\int_0^\infty\gamma(r)rJ_0(kr)dr\geqslant 0 \quad \forall k,$$

where $\gamma(r)=S_2(r)-\phi_1^2$ and $J_0(x)$ is the zeroth-order Bessel function of the first kind.

There are many other statistical correlation functions that one can employ. Indeed, the lineal-path function, $L^{(i)}(\mathbf{r}_1,\mathbf{r}_2)$ has been used to reconstruct model and actual material images.[5–8,10] This function is defined as the probability that the entire line segment joining randomly chosen points $\mathbf{r}_1$ and $\mathbf{r}_2$ lies in the same phase i. Thus, it contains connectedness information along a lineal path. If the medium is statistically homogeneous, then $L^{(i)}$ depends only on $\mathbf{r}=\mathbf{r}_1-\mathbf{r}_2$. Moreover, if the medium is statistically isotropic, then $L^{(i)}(r)$ depends on the distance $r=|\mathbf{r}|$. Hereafter, we will drop the superscript and refer to $L(\mathbf{r})$ as the lineal-path function of phase 1. At its extreme values, $L(\mathbf{r})$ is given by

$$\lim_{r\to 0}L(\mathbf{r})=\phi_1, \quad \lim_{r\to\infty}L(\mathbf{r})=0. \tag{8}$$

Recently, the pore-size distribution function was also used to reconstruct sandstones.[10]

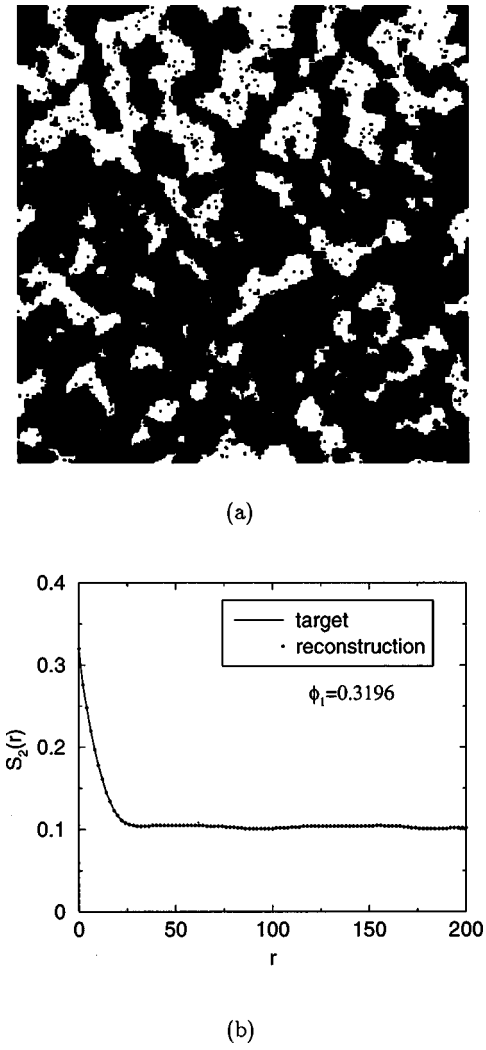

FIG. 2. (a) Reconstruction of the image shown in Fig. 1(a). The following parameters are used: $T_0=5\times10^{-5}$, $\lambda_{MC}=10$, $\lambda=0.9$, and the image size is 400×400 pixels. (b) Autocorrelation function $S_2(r)$ vs r: solid line is the target function and circles represent the reconstructed function.

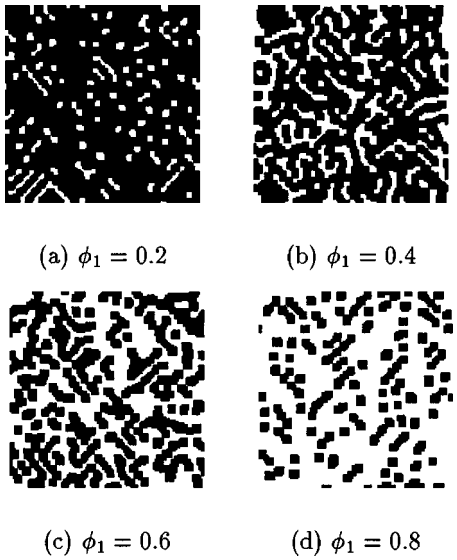

FIG. 3. Construction of structures having the autocorrelation function given by Eq. (11), at different values of ϕ_1, in which $r_0=16$ and $a_0=8$. Construction is implemented on a square grid by optimizing in two orthogonal directions. The following parameters are used: system size is 128×128 pixles, $T_0=1\times10^{-4}$, $\lambda_{MC}=10$, and $\lambda=0.9$.

III. STOCHASTIC OPTIMIZATION PROCEDURE

We briefly outline the stochastic optimization technique used to reconstruct or construct digitized media.[5] It is desired to reconstruct a target system of a given size with its known correlation functions or construct a system with some targeted correlation functions. The simulation begins with an initial guess for the configuration of phase 1 (white) and phase 2 (black) pixels for a given system size. For example, one can start with a random guess: white and black pixels are assigned with probability ϕ_1 and ϕ_2, respectively. Because the system is of finite size, this process could lead to the initial microstructure having an actual ϕ_2 value different from the desired ϕ_2 value. In practice, the number of black pixels n_b is first calculated and then n_b of the total number of pixels in the system are randomly assigned to be black. The remaining pixels are assigned to be white.

White and black pixels are interchanged so that the system evolves toward the target correlation functions via simulated annealing. The ''energy'' E at any time step in the simulation is calculated by[5]

$$E=\sum_{\mathbf{r}_1,\mathbf{r}_2,\ldots,\mathbf{r}_n}\sum_{\alpha}[f_n^{\alpha}(\mathbf{r}_1,\mathbf{r}_2,\ldots,\mathbf{r}_n)-\tilde{f}_n^{\alpha}(\mathbf{r}_1,\mathbf{r}_2,\ldots,\mathbf{r}_n)]^2, \tag{9}$$

where f_n^{α} and $\tilde{f}_n^{\alpha}$ are the simulated and targeted n-point functions, respectively, and α denotes the type of correlation function. At each time step, a randomly chosen white pixel is interchanged with a randomly chosen black pixel. The acceptance probability P for this interchange is given by the Boltzmann probability

$$P(E_{\text{old}}\rightarrow E_{\text{new}})=\begin{cases}1 & \text{if } \Delta E<0,\\ e^{-\Delta E/T} & \text{if } \Delta E\geqslant 0,\end{cases} \tag{10}$$

where $\Delta E=E_{\text{new}}-E_{\text{old}}$ and T is a fictitious temperature. The temperature T is initially chosen so that the initial acceptance probability for a pixel interchange with $\Delta E\geqslant0$ is 0.5. By slowly cooling the system to absolute zero, the system equilibrates to its ground state, i.e., the energy is minimized (target correlation functions are attained). In the reconstructions that follow, $\alpha=1$ and f_2^1 is either S_2 or L. For a more complete description of this algorithm, we refer the reader to Refs. 4–7.

IV. RECONSTRUCTION OF CERAMIC-METAL COMPOSITE

We first consider an image of an actual isotropic, interpenetrating ceramic-metal composite for which the autocorrelation function $S_2(r)$ is essentially a decaying exponential without any short-range order.[11] The function $S_2(r)$ can be obtained by ''throwing'' down line segments of length r with random orientation and counting the fraction of times that both end points fall in phase 1. To reduce computational cost, one can sample $S_2(r)$ only along rows and columns of the underlying lattice.[5] Thus, it is only in these orthogonal

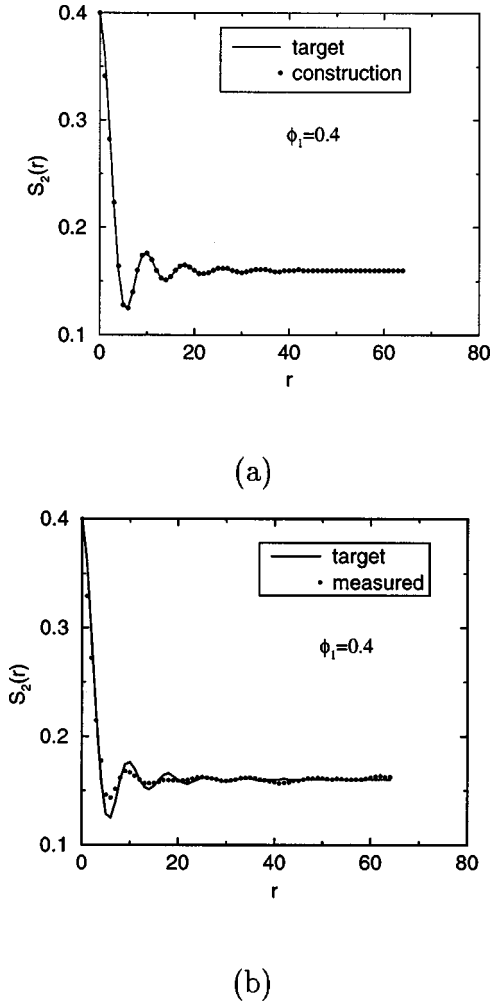

FIG. 4. (a) $S_2(r)$ vs r for the image shown in Fig. 3(b) with $\phi_1=0.4$: solid line is the target function and circles represent the constructed function. (b) $S_2(r)$ vs r as found by sampling the constructed image in Fig. 3(b) in all directions.

directions that $S_2(r)$ actually matches the target function at the end of the optimization process. For this reason, we call the sampling directions the *optimized* directions. We will demonstrate that the orthogonal sampling method results in a reasonable reconstruction of the ceramic-metal composite-free of any artificial anisotropic effects.

A two-phase image of the ceramic-metal composite is shown in Fig. 1(a). The white phase (phase 1) is aluminum. The black phase (phase 2) is a ceramic phase composed mainly of boron carbide. The image is 612×482 pixels. The measured autocorrelation function of the image, shown in Fig. 1(b), displays no appreciable short-range order.

Figure 2(a) shows the reconstructed image using S_2 and the orthogonal sampling technique on a square grid. The parameters used in the reconstruction are $T_0=5\times10^{-5}$, $\lambda_{\mathrm{MC}}=10$, $\lambda=0.9$, and the system size is 400×400 pixels. The resulting autocorrelation function is presented in Fig. 2(b) along with the target data for comparison. As can be seen, the S_2 function for the reconstructed image matches the target S_2 function virtually perfectly. The initial energy of the system is 0.2. The reconstruction is stopped when the energy reaches a value of 1×10^{-8}. Note that by the time the energy reaches a value of 1×10^{-7}, the essential structure of the original image has been captured in the reconstruction.

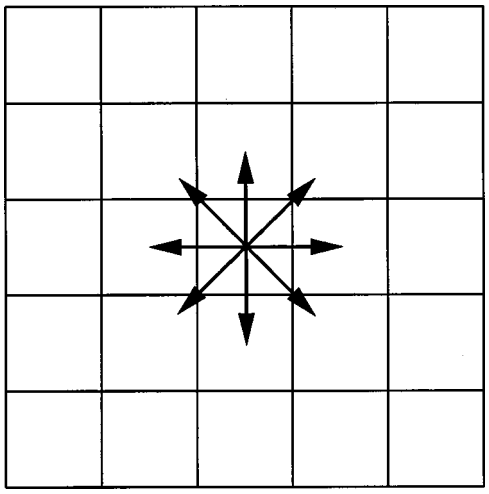

FIG. 5. Square grid showing the four directions the autocorrelation function is simultaneously optimized in.

V. BETTER SAMPLING PROCEDURES

To show that the orthogonal sampling technique on a square grid is insufficient to construct isotropic images with significant short-range order, Cule and Torquato[7] introduced the isotropic autocorrelation function

$$S_2(r)=\phi_1^2+\phi_1\phi_2 e^{-r/r_0}\,\frac{\sin(kr)}{kr}, \tag{11}$$

where $k=2\pi/a_0$. The parameters a_0 and r_0 correspond to two distinct length scales. The parameter r_0 controls the exponential damping, which determines the maximum correlations in the system. The constant a_0 controls the oscillations in the term $\sin(kr)/(kr)$ which also decays with increasing r such that a_0 can reduce the effective range of r_0. The positivity conditions (7) determine the allowable range of the parameters a_0 and r_0.[9]

Figure 3 shows images at different volume fractions having the autocorrelation function (11), which we constructed using orthogonal sampling on a square grid. For all of the images shown, the constructed and target autocorrelation functions match very well. One such plot is shown in Fig. 4(a). Importantly, the autocorrelation function sampled from the constructed image at 45° with respect to the horizontal (not shown) does not match the targeted function. This mismatch is also indicated in Fig. 4(b), where we measured S_2 from the constructed image by sampling in *all* directions. Thus, the constructed image contains unwanted statistical anisotropy, otherwise there would be no mismatch.

It is important to emphasize that for a statistically isotropic image, it is acceptable to sample for the correlation functions in two orthogonal directions only. However, when one attempts to *construct* an image with an isotropic correlation function displaying appreciable short-range order, it is not sufficient to optimize in only two directions.

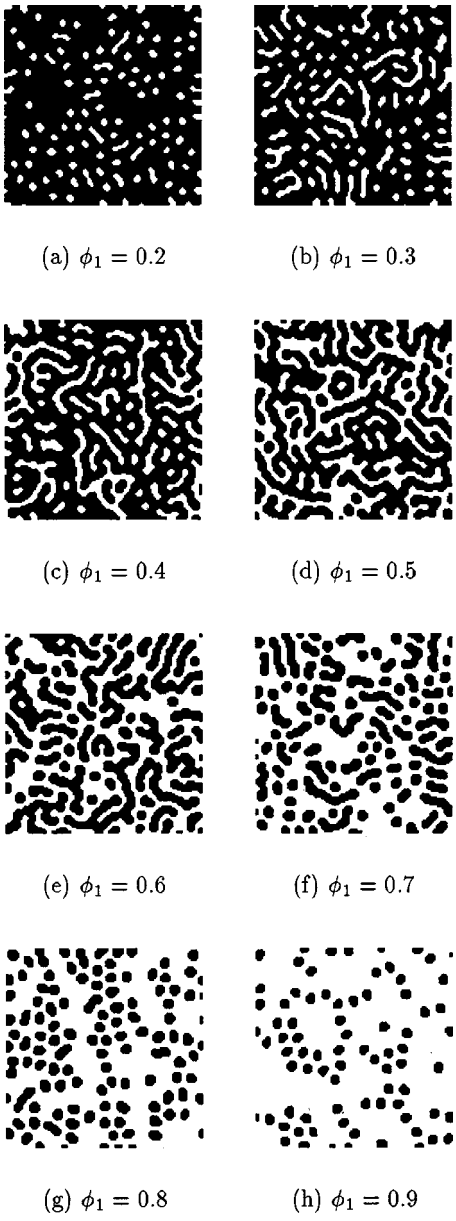

FIG. 6. Construction of structures having the autocorrelation function given by Eq. (11), at different values of ϕ_1, in which $r_0=16$ and $a_0=8$. Construction is implemented on the square grid by optimizing in four directions as shown in Fig. 5. The following parameters are used: system size is 128×128 pixels, $T_0=1\times10^{-4}$, $\lambda_{MC}=10$, and $\lambda=0.9$.

A. Square grid sampling in four directions

In cases where there is appreciable short-range order, one needs to increase the number of sampling directions over which the system is optimized. A natural improvement on the orthogonal sampling on a square grid is to optimize in more than two directions. Here we simultaneously optimize in four directions. The square grid and the sampling directions for the autocorrelation function are shown in Fig. 5. Images are constructed using Eq. (11) as the target function and optimized in four directions. The constructed images are shown in Fig. 6. The parameters used in this construction are as follows: the system size is 128×128 pixels, $T_0=1\times10^{-4}$, $\lambda_{MC}=10$, and $\lambda=0.9$. The constructed and targeted functions (not shown) were found to match essentially perfectly.

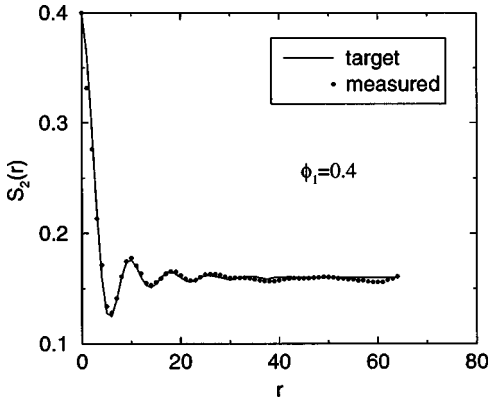

FIG. 7. $S_2(r)$ vs r as found by sampling the constructed image in Fig. 6(c) in all directions.

To test for anisotropy, we measured S_2 from the constructed images by sampling in the unoptimized directions and found that they matched the targeted autocorrelation functions. This shows that by increasing the number of directions being simultaneously optimized, we eliminate unwanted anisotropy in the constructed image. Figure 7 gives a plot of $S_2(r)$ versus r at $\phi_1=0.4$ as measured from the constructed image of Fig. 6(c) by sampling in all directions. Clearly, the artificial anisotropic effects have been completely removed. This is in contrast to optimizing in only two orthogonal directions, which yields a mismatch, as shown for example in Fig. 4(b).

B. Hexagonal grid

Let us now consider a regular hexagonal tessellation of 2D space, henceforth referred to as a hexagonal grid. This choice enables the autocorrelation function to be simultaneously optimized in the three symmetry directions, which should also lessen the artificial anisotropic effects. Figure 8 shows the hexagonal grid and the sampling directions. It also shows how the unit cell repeats in the vertical direction and also in the horizontal direction. Such a unit cell is chosen because it is a convenient way to implement the periodic boundary conditions. It should be noted that different boundary conditions will result if an odd system size is chosen. Therefore, we have restricted the system size to be even.

We construct the image by optimizing in the three symmetry directions on the hexagonal grid. Here the system size is 128×128 pixels, $T_0=1\times10^{-4}$, $\lambda_{MC}=10$, and $\lambda=0.9$. The constructions are shown in Fig. 9. By sampling the constructed image for the autocorrelation function in the unoptimized directions (not shown), it is again found that the measured function matches the targeted function. Thus, artificial anisotropic effects have been removed by sampling in three directions on a hexagonal grid.

At small values of ϕ_1, the constructed system is a dispersion of phase 1 particles in a black matrix. At intermediate values of ϕ_1 the microstructure is labyrinthine like. At high values of ϕ_1, the constructed system is a dispersion of

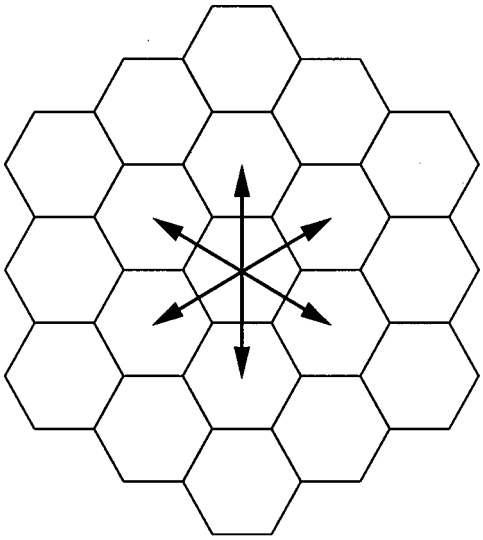

(a)

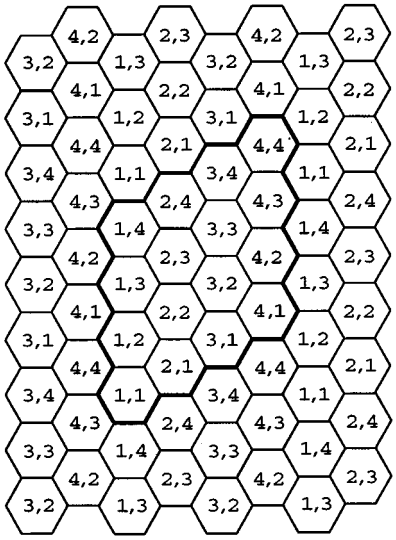

(b)

FIG. 8. Hexagonal grid used in the reconstruction technique. (a) Sampling directions. (b) The unit cell is shown in bold and the surrounding cells are included to explain the implementation of the periodic boundary conditions. The pixel labeling is explained as follows: the first index indicates the column number and the second index indicates the row number of the pixel.

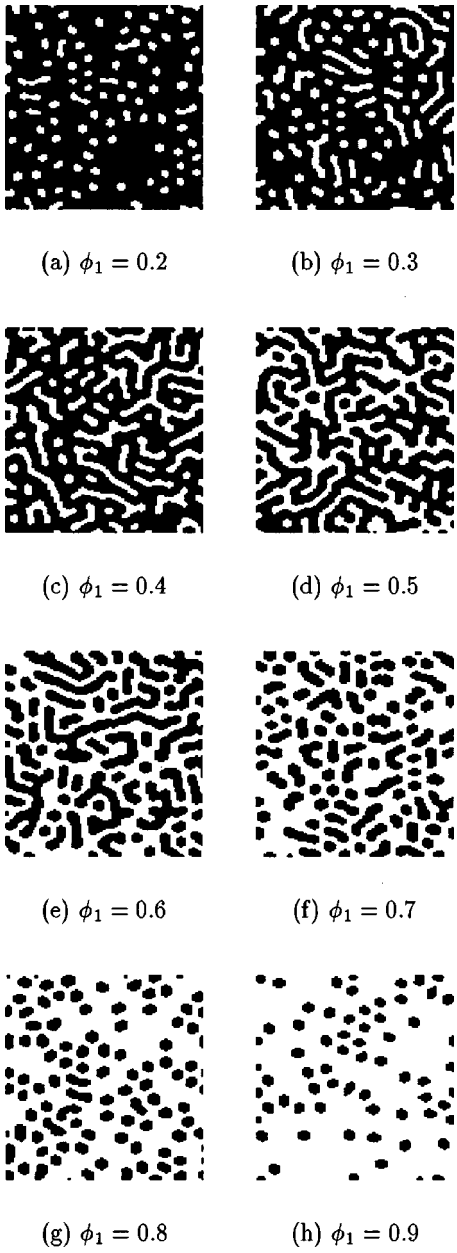

(a) $\phi_1 = 0.2$ (b) $\phi_1 = 0.3$

(c) $\phi_1 = 0.4$ (d) $\phi_1 = 0.5$

(e) $\phi_1 = 0.6$ (f) $\phi_1 = 0.7$

(g) $\phi_1 = 0.8$ (h) $\phi_1 = 0.9$

FIG. 9. Construction of structures having the autocorrelation function given by Eq. (11), at different values of ϕ_1, in which $r_0 = 16$ and $a_0 = 8$. Construction is implemented on the hexagonal grid shown in Fig. 8 by optimizing in three directions. The following parameters are used: the system size is 128×128 pixels, $T_0 = 1 \times 10^{-4}$, $\lambda_{MC} = 10$, and $\lambda = 0.9$.

phase 2 particles in a white matrix. Figure 10(a) shows a typical plot of the target and system autocorrelation functions, which are in excellent agreement with each other.

C. Comparison of improved sampling procedures

Let us now compare the construction results for the hexagonal grid and the square grid where we optimize in four directions. Both methods give very similar images and in terms of the agreement between the autocorrelation functions of the target and constructed images.

Of course, optimizing on the hexagonal grid is faster since one only has to optimize in three directions. Also, optimizing in four directions on a square grid is inefficient. For the square grid, when the sampling radius increases by one pixel we are guaranteed to move to another pixel in the horizontal and vertical direction. However, in the diagonal directions, where a distance of $\sqrt{2}$ pixels is required to move to another pixel, it is common to increase the sampling radius by one pixel and still sample the same pixel. At any rate, sampling on a hexagonal grid in three directions is preferred over sampling on a square grid in four directions. However, sampling on the square grid is easier to implement.

VI. NONUNIQUENESS

We will now address an issue concerning the nonuniqueness of the reconstructed images. It has been shown that

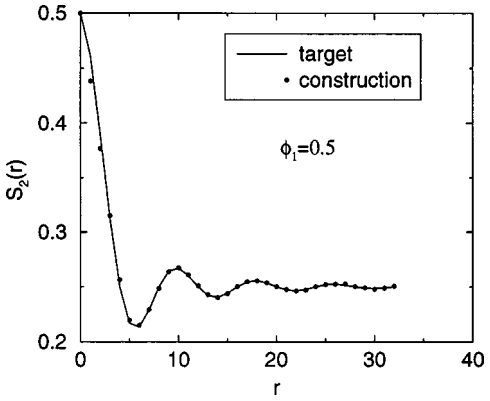

FIG. 10. A plot of S_2 vs r for the image shown in Fig. 9 with $\phi_1=0.5$: solid line is the target function and circles represent the constructed function.

higher-order correlation functions are typically not sufficient to (re)construct an image perfectly.[5,7] This was demonstrated by reconstructing an image using the autocorrelation function only and then showing that the lineal-path function of the resulting image differs from the expected lineal-path function.

We examine the variability in the untargeted correlation functions by choosing different initial conditions. To do this, we will reconstruct a one-dimensional ''overlapping-rod'' system. Figure 11 shows one such realization of an overlapping-rod system which is generated by randomly placing rods of length 10 pixels on a line of 1000 pixels until the black phase area fraction (area fraction of the rods) is $\phi_2=0.5$. The analytical autocorrelation function for this system is[12]

$$S_2(r)=\exp\left(-\eta\frac{v_2(r;R)}{v_1(R)}\right), \tag{12}$$

where

$$\frac{v_2(r;R)}{v_1(R)}=2\Theta(r-2R)+\left(1+\frac{r}{2R}\right)\Theta(2R-r). \tag{13}$$

$2R$ is the rod length, $\eta=-\ln(\phi_1)$, and $\Theta(x)$ is the Heaviside step function [$\Theta(x)=1$ if $x>0$ and $\Theta(x)=0$ if $x<0$]. The analytical relation for L for this system is given by[13]

$$L(r)=\phi_1^{1+r/(2R)}, \tag{14}$$

where R is the rod length as given earlier.

First, the system is reconstructed using only the autocorrelation function as the target. The lineal-path function of the reconstructed image is then measured. Three different reconstructed images are generated using three different initial guesses (seed values for the random number generator), one of which is shown in Fig. 12(a). Figure 12(b) shows how the analytical autocorrelation function agrees with the measured

FIG. 11. Realization of an overlapping-rod system: The system size is 1000 pixels. The rod length is 10 pixels and the area fraction of phase 1, $\phi_1=0.5$.

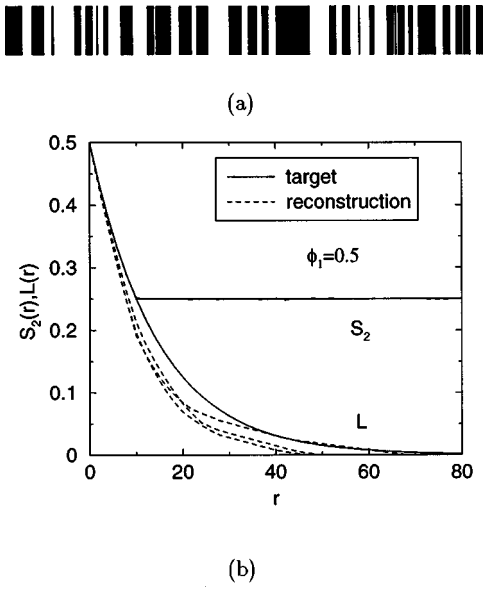

FIG. 12. (a) Reconstruction of the overlapping rod system using the autocorrelation function as the target function, for a system size of 1000 pixels. (b) $S_2(r)$ vs r for a system size of 1000 pixels: solid line is the target function and dashed line represents the reconstructed image. Both lines are indistinguishable from each other. $L(r)$ vs r measured for the three reconstructions is also shown: the solid line is the analytical function and the dashed line represents the measured function.

S_2 function. It also shows how the lineal-path function of the reconstructed image differs from the theoretical function: an indication of the nonuniqueness of the reconstruction. Indeed, there is variability in the lineal-path function from one reconstruction to another.

The process is then conducted in reverse, i.e., the reconstruction uses the analytical lineal-path function as the target

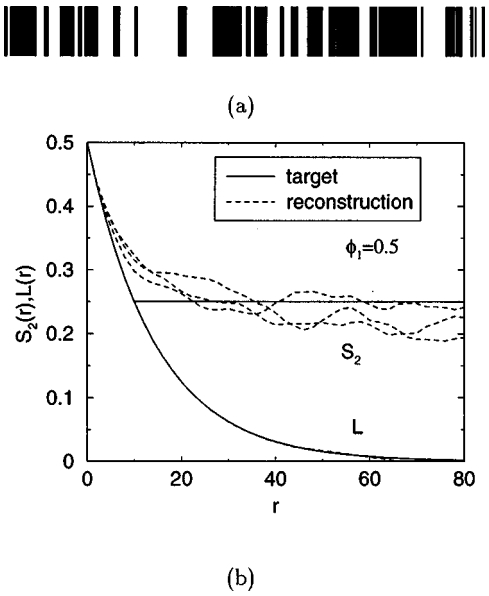

FIG. 13. (a) Reconstruction of the overlapping-rod system using the lineal-path function as the target function, for a system size of 1000 pixels. (b) $L(r)$ vs r for a system size of 1000 pixels: solid line is the target function and the dashed line represents the reconstructed image. Both lines are indistinguishable from each other. $S_2(r)$ vs r measured for the three reconstructions is also shown: the solid line is the analytical function and the dashed line represents the measured function.

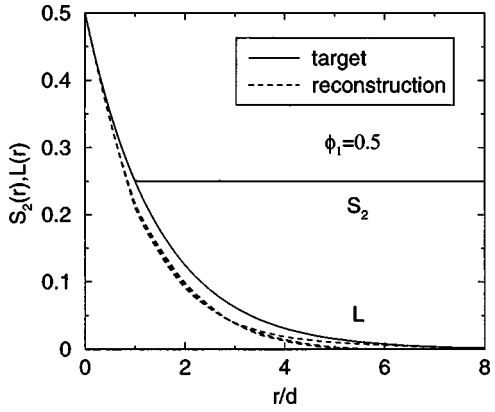

FIG. 14. $S_2(r)$ vs r for a system size of 10 000 pixels: solid line is the target function and the dashed line represents the reconstructed image. Both lines are indistinguishable from each other. $L(r)$ vs r measured for the three reconstructions is also shown: the solid line is the analytical function and the dashed line represents the measured function.

and the resulting S_2 function is then measured. Figure 13 shows the results of the reconstructions. Again, there is excellent agreement between the analytical lineal-path function and the measured function. There is, however, significant variability in autocorrelation functions between the different reconstructions. Moreover, they do not reach their long range value of ϕ_1^2.

An important question is the following: How much of this variability is simply due to finite-size effects? To answer this question, we increase the system size by a factor of 10 to 10 000 pixels, and then we reconstruct the overlapping rod system again using three different initial guesses and using S_2 as the target function. The lineal-path function L, is then measured for the resulting reconstructed images. The results are shown in Fig. 14. One can see that the lineal-path functions sampled from the reconstructed image are converging to one curve and, thus, the variations are attributable to finite-size effects. Therefore, when probing for nonuniqueness by the measurement of untargeted correlation functions, one should minimize finite-size effects.

It should be noted that Yeong and Torquato[6] showed that by using both S_2 and L as the target functions, the reconstructions are improved significantly.

VII. CONCLUSIONS

We have investigated further the recently developed stochastic optimization technique for reconstructing digitized random heterogeneous materials.[5,6] We have shown how the orthogonal sampling technique can successfully reconstruct images that have autocorrelation functions that display no appreciable short-range order. However, it is known that this time-saving technique displays artificial anisotropic effects when the autocorrelation function reflects significant short-range order. To minimize such artifacts, we introduced improved sampling procedures that increase the number of sampling directions being simultaneously optimized. By sampling in three directions on a hexagonal grid or in four directions on a square grid, unwanted anisotropic effects were effectively eliminated. Among the two improved sampling procedures, sampling on a hexagonal grid is preferred. We also addressed the following nonuniqueness question: How much of the variability in untargeted correlation functions between reconstructions generated from different initial guesses is attributable to finite-size effects? We showed that the variability is due entirely to finite-size effects, and thus if nonuniqueness is to be investigated, then one should minimize finite-size effects.

ACKNOWLEDGMENT

This work was supported by the Engineering Research Program of the Office of Basic Energy Sciences at the Department of Energy (Grant No. DE-FG02-92ER14275).

[1] J. A. Quibler, J. Colloid Interface Sci. **98**, 84 (1984).
[2] P. M. Adler, C. G. Jacquin, and J. A. Quibler, Int. J. Multiphase Flow **16**, 691 (1990); P. M. Adler, C. G. Jacquin, and J. F. Thovert, Water Resour. Res. **28**, 1571 (1992).
[3] A. P. Roberts and M. Teubner, Phys. Rev. E **51**, 4141 (1995).
[4] M. D. Rintoul and S. Torquato, J. Colloid Interface Sci. **186**, 467 (1997).
[5] C. L. Y. Yeong and S. Torquato, Phys. Rev. E **57**, 495 (1998).
[6] C. L. Y. Yeong and S. Torquato, Phys. Rev. E **58**, 224 (1998).
[7] D. Cule and S. Torquato, J. Appl. Phys. **86**, 3428 (1999).
[8] C. Manwart and R. Hilfer, Phys. Rev. E **59**, 5596 (1999).
[9] S. Torquato, J. Chem. Phys. **111**, 8832 (1999).
[10] C. Manwart, S. Torquato, and R. Hilfer, Phys. Rev. E **62**, 893 (2000).
[11] S. Torquato, C. L. Yeong, M. D. Rintoul, D. Milius, and I. A. Aksay, J. Am. Ceram. Soc. **82**, 1263 (1999).
[12] S. Torquato, Appl. Mech. Rev. **44**, 37 (1991).
[13] B. Lu and S. Torquato, Phys. Rev. A **45**, 922 (1992).